Int J Thermophys (2008) 29:285–300
DOI 10.1007/s10765-007-0308-6

Thermodynamic Radiation Thermometry for the Next SI

H. W. Yoon · C. E. Gibson · V. Khromchenko · G. P. Eppeldauer · R. R. Bousquet · S. W. Brown · K. R. Lykke

Published online: 15 November 2007

Abstract The construction, the calibration, and the use of the NIST Thermodynamic Radiation Thermometer (TRT) to measure the temperature of the gold freezing temperature blackbody and a variable-temperature blackbody from 800 to 2,700°C are described. These temperature determinations are detector-based and derived from the electrical substitution radiometer and length units. The TRT is constructed using a cooled, near-infrared enhanced silicon detector with a room-temperature-stabilized five-position filter wheel. The characteristics of the TRT, such as the size-of-source effect and preamplifier linearity, are determined. The measured temperatures are compared with those obtained using the NIST Absolute Pyrometer 1 (AP1) and the current NIST standard radiation thermometer, the Photoelectric Pyrometer (PEP). After the performance assessments, the TRT will become the standard radiation thermometer for disseminating radiance temperature scales in the United States.

Keywords Gold freezing temperature · Kelvin · Linearity · Radiometric temperatures · Thermodynamic temperatures

1 Introduction

Discussions are underway to base the *International System of Units* (SI) upon fundamental physical constants and, in particular, to adopt a fixed Boltzmann constant as the

H. W. Yoon (✉) · C. E. Gibson · G. P. Eppeldauer · R. R. Bousquet · S. W. Brown · K. R. Lykke
Optical Technology Division (844), National Institute of Standards and Technology, 100 Bureau Drive, Stop 8441, Gaithersburg, MD 20899-8441, USA
e-mail: howard.yoon@nist.gov

V. Khromchenko
Joint NIST/USU Program in Optical Sensor Calibration, Space Dynamics Laboratory, Utah State University, 1695 North Research Park Way, North Logan, UT 84341, USA

basis of the unit of temperature, the kelvin [1]. Thus, in the future, temperatures may be disseminated either on the basis of a practical temperature scale or by direct thermodynamic temperature measurements. These thermodynamic temperature measurements can include, among others, constant-volume gas thermometry, acoustic thermometry, noise thermometry, dielectric-constant gas thermometry, and detector-based radiation thermometry [2].

The International Temperature Scale of 1990 (ITS-90) defines temperatures above the Ag freezing temperature (961.78°C) by the use of Planck radiance ratios with respect to the Ag, Au, or Cu freezing-temperature blackbodies [3]. However, due to possible long-term material contamination and oxide formation in the freezing-point blackbodies, the lowest uncertainties can only be obtained if the fixed points are compared to each other [4,5]. At temperatures above the freezing temperature of Ag, the use of detector-based radiation thermometers can lead to lower thermodynamic temperature uncertainties than those resulting from using ITS-90 techniques [6].

There are different approaches to implementing detector-based radiation thermometry. Most commonly, the spectral irradiance responsivity of a simple filter radiometer with a broad- or narrow-band spectral filter and a precision aperture can be determined by comparison to a calibrated Si diode or a Si-trap detector [7] using a lamp-monochromator source [8,9]. These filter radiometers require a precision aperture at the source and a known distance between the two apertures to define the incident irradiance at the entrance aperture of the radiometer. Although filter radiometers calibrated for irradiance responsivity can be used to measure the thermodynamic temperatures of fixed-point crucibles, the alignment of the small blackbody opening with the filter radiometer aperture can be difficult, with additional components of error arising from possible scattering and diffraction from the edges of the small apertures. An approach promising lower uncertainties is to calibrate the radiation thermometer as a system using a spectrally-tunable monochromatic laser-irradiated sphere calibrated for spectral radiance as in the NIST Facility for Spectral Irradiance and Radiance Responsivity Calibrations using Uniform Sources (SIRCUS) [10]. The known spectral radiance from the sphere is used to calibrate the radiation thermometer for absolute radiance responsivity, which can then be used to determine the thermodynamic temperatures of blackbodies in conjunction with the Planck radiance law.

In this work, we describe the characterization and use of the NIST Thermodynamic Radiation Thermometer (TRT) to measure the temperature of the gold freezing temperature blackbody and a variable-temperature blackbody from 800 to 2,700°C. The detector-based thermodynamic temperature determination of the gold freezing temperature is compared to the NIST Absolute Pyrometer 1 (AP1), which has been in use for over 5 years [11]. The temperatures of a Thermogauge[1] variable-temperature blackbody (TGBB) from 800 to 2,700°C are measured using the TRT, AP1, and the NIST Photoelectric Pyrometer (PEP) [12]. The temperatures are determined in two different ways: detector-based radiation thermometry using the AP1 and TRT, and

[1] Certain commercial equipment, instruments, or materials are identified in this article to foster understanding. Such identification does not imply recommendation or endorsement by the National Institute of Standards and Technology, nor does it imply that the material or equipment are necessarily the best available for the purpose.

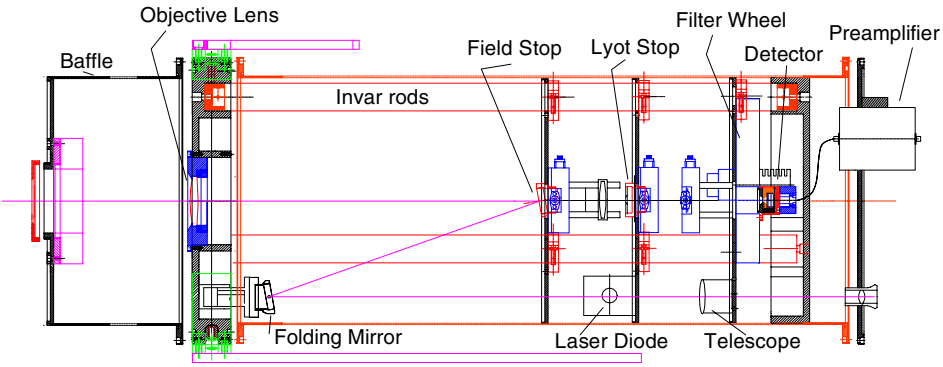

Fig. 1 NIST TRT. Diameter of the TRT is 26 cm, and the total length including the front baffle is 89 cm. Placement of the preamplifier, close to the detector and shielded by the anodized aluminum outer shell, reduces noise and electromagnetic pickup

ITS-90 based radiance ratios using the PEP with a constant-current vacuum strip lamp as a stability-check standard.

2 Experimental Setup

2.1 NIST Thermodynamic Radiation Thermometer

The physical construction of the TRT is schematically shown in Fig. 1. The specifications of the TRT are listed in Table 1. The optical components are fixed with three Invar rods for structural stability, and all the remaining parts are machined from aluminum and black-anodized to reduce scatter and reflections. The use of the anodized aluminum outer case is to ensure thermal stabilization of the internal components to the laboratory surroundings. The TRT detector is a 5.8 mm by 5.8 mm near-infrared enhanced silicon detector that is thermo-electrically cooled to −25°C. The spectral selection is achieved using a thermally-stabilized five-position filter wheel, which is held at 30°C. The temperature of the filter wheel was stable at temperatures above ambient, but could not be made stable if the temperature were held below ambient. The TRT utilizes an on-axis 50 mm diameter, 200 mm focal length achromatic lens selected for low scatter. The field stop of the TRT is tilted such that the specular reflection is directed at a folding mirror and viewed through the internal magnifying telescope. The specular reflection from the metallic surface of the field stop is sufficient to be useful for alignments. The tilt of the field stop also reduces specular reflection back into the objective lens to reduce the size-of-source effect (SSE). There is also an alignment laser directed into the viewing axis of the telescope by a beam splitter, which provides a guide to the optical axis of the TRT. The design of the TRT enables alignment to small, <6 mm diameter fixed-point cavity openings, and alignment to <2 mm wide tungsten strip lamps.

Table 1 TRT parameters and design specifications

Object distance	50 cm
Image distance	33.3 cm
Objective focal length	20 cm
Field stop diameter	0.6 mm
Target diameter	0.9 mm
f/#	12
Lyot stop diameter	5 mm
Detector type	Near-infrared enhanced Si
Detector size	5.8 mm × 5.8 mm
Detector temperature	−25°C
Number of filters	5
Filter wheel temperature	30°C
Collimator lens focal length	70 mm
Image diameter on detector	5.0 mm
TRT diameter	26 cm
TRT length	89 cm

Table 2 Gain ratios obtained using a stable LED source

Gain ratios are referenced to a gain of 10^9 V·A^{-1} where the detector-based radiance responsivity calibrations are performed in the SIRCUS facility

TRT gain settings	Gain ratios to 9
5	0.9981×10^{-4}
6	0.9983×10^{-3}
7	0.9984×10^{-2}
8	0.9985×10^{-1}
9	1.0000
10	1.0006×10^{1}

2.1.1 Preamplifier Performance and Linearity

The linearity of the TRT preamplifier gain settings was determined using a variable-intensity LED source. The source intensity was changed, and then measured at different gain settings of the preamplifier. The preamplifier was constructed using high precision resistors with tolerances of <0.05% ($k = 1$) in gain ranges of 10^3–10^8 V·A^{-1} and tolerances of <0.5% ($k = 1$) in gain ranges of 10^9 and 10^{10} V·A^{-1}. The temperature dependencies of the resistances in the same ranges are 10×10^{-6} and $100 \times 10^{-6}\Omega \cdot \Omega^{-1} \cdot °C^{-1}$, respectively. The measured gain ratios in Table 2 are in agreement with the above specifications. For example, the gain ratios for the preamplifier range of 10^5 to 10^8 V·A^{-1} change by <0.05%, while there is a larger increase with 10^9 V·A^{-1}. In Table 2, the gains are given as ratios with respect to the gain at 10^9 V·A^{-1} since the system-level radiometric calibrations were performed at this gain setting.

2.1.2 Size-of-Source Effect

The SSE was measured using a central obscuration attached to ground-glass plates placed in front of an LED source [13] with a variable-diameter iris to change the outer diameter of the LED source. The TRT was designed to have a minimal SSE since the uncertainty of the SSE can dominate for the lowest uncertainty measurements. With

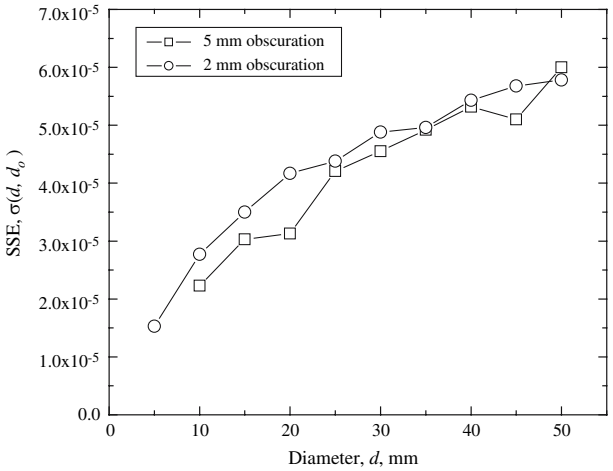

Fig. 2 SSE of the TRT650 expressed using Eq. 1 with 2 and 5 mm central obscurations attached to the LED source. A variable-diameter iris was used to change the outer diameter of the LED source

the selection of a low-scatter objective lens and the implementation of the Lyot stop along with the tilt of the field stop, the TRT is measured to have a SSE of $<6 \times 10^{-5}$ when measuring a source of 50 mm diameter with a central obscuration of 2 or 5 mm diameter, as shown in Fig. 2. The SSE is plotted in Fig. 2 using

$$\sigma(d, d_o) = \frac{v(L, d) - v(L, d_o)}{v(L)}, \tag{1}$$

where d is the diameter of the uniform radiance source, d_o is the diameter of the central obscuration, and L is the radiance of the source. The signal measured while viewing the unobstructed radiance source is $v(L)$, and the signal measured while viewing the central obscuration with the diameter of the radiance source, d, is $v(L, d)$. The signal measured with the diameter of the variable aperture at the diameter of the central obscuration, d_o, is $v(L,d_o)$. This generalized approach to reducing the SSE can lead to reproducible construction of radiation thermometers with low SSE [14,15].

2.1.3 Modeling of Optical Performance

Since the TRT is designed with a five-position filter wheel and a near-infrared enhanced Si diode with power sensitivity to 1,000 nm, the focal shift and the imaging performance at a wide range of wavelengths were modeled in order to utilize the TRT at a wide range of wavelengths. Use of narrow spectral-width bandpass filters from 400 to 1,000 nm will enable the TRT to be used to determine the spectral emissivity of blackbodies, and the use of broad bandpass filters will enable measurement of a wide range of blackbody temperatures down to 400°C. The chromatic focal shift of the achromat objective lens, shown in Fig. 3, reflects the use of two optical elements cemented into a doublet. Since the original design of the achromat optimized

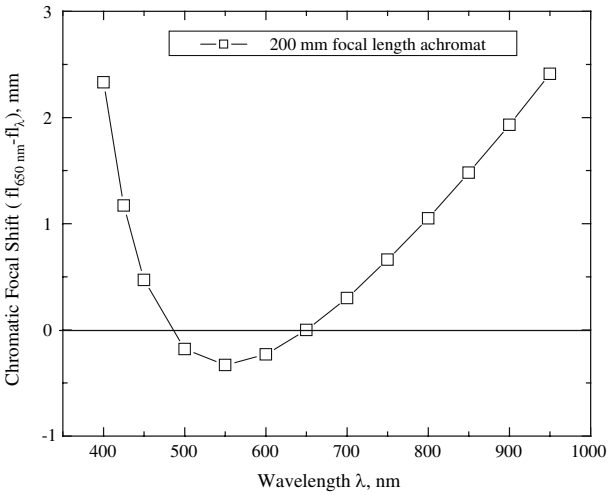

Fig. 3 Chromatic focal shift of the achromatic objective lens in the TRT. The focus shifts a few mm from the nominal 333 mm image distance from the objective lens to the field stop

performance for the visible wavelengths, the wavelength of minimum curvature is at 550 nm, corresponding to the maximum of the photopic response. The chromatic focal shift introduces a few mm offset between the optimum focus at an image distance of ∼333 mm. Due to the small, 0.9 mm target diameter, the chromatic focal shift should not introduce a significant distance effect with wavelength, especially when viewing targets or blackbody openings that are significantly larger than the target diameter. The chromatic focal shift can be accommodated by a shift of the object distance into the blackbody opening. Since high-quality blackbodies are lambertian and spatially uniform, this focus shift will not lead to a significant change in the measured signal beyond the combined uncertainties.

2.1.4 Detector-Based Radiance Responsivity

The detector-based radiance responsivity of the TRT 650 nm channel was measured in the NIST SIRCUS facility, as shown in Fig. 4. The radiance responsivity is similar to the AP1 since the same ion-assisted deposited filter is used for the TRT650 as for the AP1. The slight differences in the radiance responsivities from the AP1 are due to the use of a near-infrared suppressed Si diode in the AP1 as compared to the near-infrared enhanced Si diode in the TRT. Even with the use of only a single filter, the out-of-band suppression from the peak responsivity is $>10^{-7}$ toward the longer wavelength side of the peak. This suppression is especially important for the measurement of blackbodies at temperatures around the gold freezing temperatures, where the Planck radiance increases by >100 in the longer wavelength region from 650 to 1,000 nm. The uncertainties of the TRT650 radiance responsivities will be discussed in a later section.

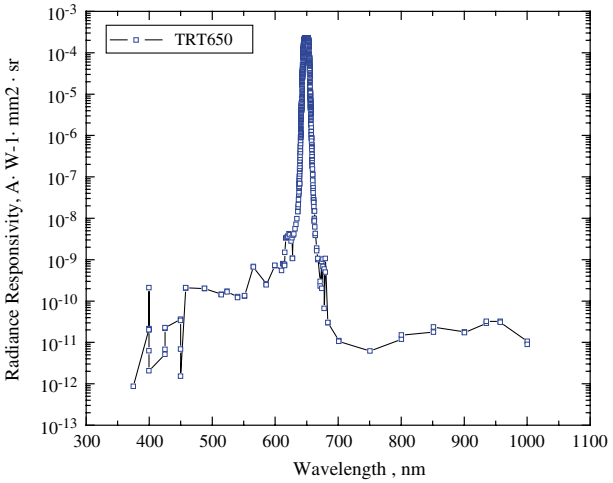

Fig. 4 Detector-based radiance responsivity of the TRT650 measured in the NIST SIRCUS facility

The detector-based radiance responsivities are converted to calculated photocurrents, i_c, by

$$i_c = \int S_L L\,(\lambda, T)\,\mathrm{d}\lambda, \tag{2}$$

where S_L is the absolute radiance responsivity, and $L(\lambda, T)$ is the spectral radiance given by the Planck radiance law. The Planck radiance law is given by

$$L(\lambda, T) = \frac{c_{1L}}{n^2\lambda^5} \frac{1}{\exp\left(c_2/\left(n\lambda T\right)\right) - 1}, \tag{3}$$

where c_{1L} and c_2 are the first and second radiation constants, T is the thermodynamic temperature, λ is the wavelength of the radiation in air, and n is the refractive index. For these calculations, the CODATA values [16] for the radiation constants and the refractive index of air of $n = 1.00029$ were utilized. The calculated photocurrents in Fig. 5 show that the range of temperatures from 800°C to beyond 3,000°C can be measured with the TRT650. After the radiance responsivities of the other channels are determined, similar current to temperature relationships will be obtained.

2.2 PEP

Since the early 1990s, the NIST Photoelectric Pyrometer has been the standard radiation thermometer for the dissemination of radiance temperature scales above the freezing temperature of silver. Briefly, the PEP is operated as a spectral radiance comparator of a stable vacuum tungsten-ribbon-filament lamp (RFL) and the variable-temperature blackbody (VTBB). The radiance temperature of the RFL is assigned from the gold freezing temperature blackbody using the PEP, and the RFL is then used as the

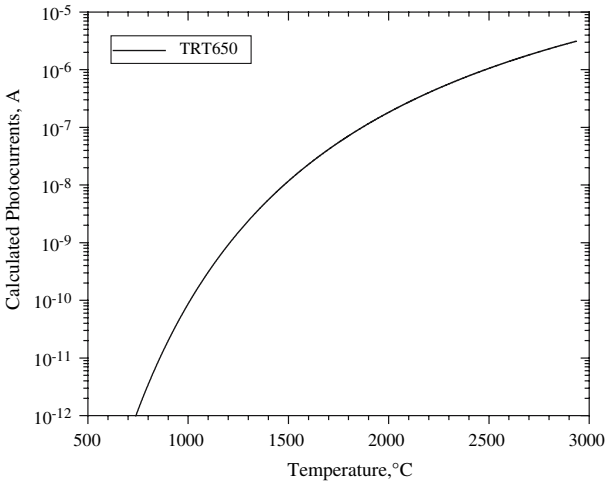

Fig. 5 Calculated photocurrents of the TRT650 found using Eq. 2. Corrections for gain, linearity, blackbody emissivity, and SSE are applied to the measured photocurrents

calibrated working standard for radiance temperature assignment of the VTBB. The PEP is constructed using a singlet objective lens with a field stop to view a 0.6 mm by 0.8 mm target. The spectral selection is performed using two interference filters with about 3 nm bandwidth centered at 655 nm. A photomultiplier tube (PMT) is used as the detector. The PMT cannot be used over the entire temperature range from 800 to 2,700°C without changing the high voltage setting and relies on the long-term stability of the RFL for its calibration. Further information can be found in [12].

2.3 AP1

The AP1 has been described in previous publications [11]. Since we have a long history of detector-based calibrations with the AP1, the new radiation thermometer, the TRT650, was compared to the AP1 determinations of the gold freezing blackbody and temperature measurements of the variable temperature blackbody using the other two radiation thermometers. With the repeat radiance responsivity measurements in SIRCUS and of the gold freezing temperature blackbody, the estimated uncertainties of the detector-based calibrations can be tested with the AP1. Since the gold freezing temperature blackbody is found to be reproducible to <38 mK ($k = 2$) [17], any deviations of the measured signals of the radiation thermometers outside this limit are expected to be due to changes in the radiation thermometer or its alignment. The SIRCUS calibrations of the radiance responsivities of the AP1 over a period of $3\frac{1}{2}$ years are shown in Fig. 6. The spectral range is limited to 649–651 nm to closely examine the changes in the radiance responsivity over this time period. While there was a rapid decrease in the responsivities from June 2003 to March 2005, the radiance responsivities are shown to be reproducible from March 2005 to November 2006. These SIRCUS measurements include changes in the internal SIRCUS scales from

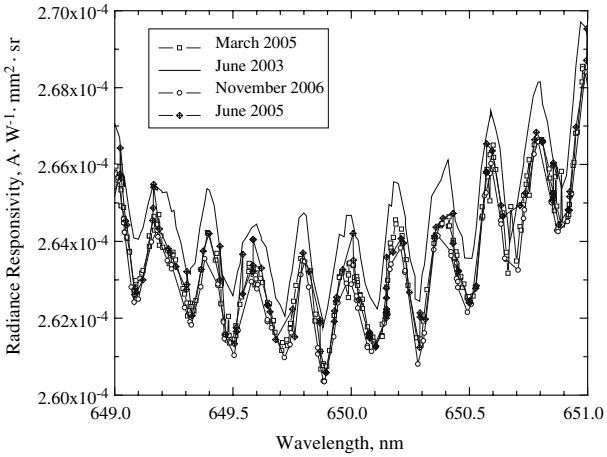

Fig. 6 SIRCUS radiance responsivity measurements of the AP1 on the respective dates. Each measurement requires separate independent alignment and setup of the SIRCUS equipment, and thus tests the reproducibility of the calibrations

Table 3 Detector-based calculated photocurrents for the AP1 calibrations in SIRCUS performed on the respective dates

Date of SIRCUS calibration	Gain	AP1 calculated gold-point current (A)
November 2006	9	1.644297×10^{-10}
June 2005	8	1.646697×10^{-10}
March 2005	8	1.646799×10^{-10}

Table 4 AP1 gain factor ratios as compared to the ratios of the SIRCUS calibrations

AP1 gains	AP1 gain factor ($V \cdot A^{-1}$)	Gain factor ratio (8/9)	Ratio of calculated gold-point currents (June 05/Nov. 06)
8	9.96020×10^7	1.00121	1.00146
9	9.94820×10^8		

The different gains used in the SIRCUS calibrations, as seen in Table 3, are reflected in the ratios of the calculated gold-point currents

realizations of the trap detectors against the cryogenic radiometers in the intervening time, and also include realignment of the AP1 and the reference trap detectors in the SIRCUS facility. For a more quantitative assessment, the calculated photocurrents at the freezing point of gold are listed in Table 3. The AP1 was calibrated in SIRCUS at a gain of 10^8 $V \cdot A^{-1}$ in 2005 and at a gain of 10^9 $V \cdot A^{-1}$ in 2006. The comparison of the ratios of the calculated photocurrents to the ratios of the electrical gain factors in Table 4 indicates that the differences are within the SIRCUS uncertainties and can be explained by the differences in the gain factors.

Table 5 Total uncertainty of the radiance responsivity calibrations in the NIST SIRCUS facility broken down into the component uncertainties

	SIRCUS uncertainty components ($k = 1$)	Type	(%)
1	Trap responsivity	B	0.013
2	Aperture area	B	0.002
3	Distance	B	0.005
4	Sphere spatial and angular uniformity	B	0.025
5	Amplifier gain	A	0.005
6	Temperature coefficient of trap	B	0.002
7	Temporal stability of trap	B	0.013
	Combined standard uncertainty ($k = 1$)		0.032
	Expanded uncertainty ($k = 2$)		0.063

Trap refers to the Si-diode trap detector used for the realization

3 Detector-Based Radiation Thermometer Uncertainties

3.1 Radiance Responsivity Uncertainties

Before the detector-based and ITS-90 determinations of the gold freezing temperature and VTBB temperatures can be compared, the uncertainties of the detector-based thermodynamic temperatures should be examined. The uncertainties of the detector-based radiance responsivities measured in the SIRCUS facility are listed in Table 5. The repeat calibrations, as listed in Table 4, are within the combined uncertainties listed in Table 5. Further information on these uncertainties can be obtained from [10].

3.2 Uncertainties of the Gold Freezing Temperature Determinations

The uncertainties of the thermodynamic temperature determinations of the gold freezing temperature are listed in Table 6. The component standard uncertainties are listed as percentages of the signal, and are then converted to temperature uncertainties by differentiating the Wien approximation to obtain the sensitivity coefficient,

$$\frac{\mathrm{d}L}{L} = \frac{\mathrm{c}_2}{\lambda}\frac{\mathrm{d}T}{T^2}, \tag{4}$$

where L is the radiance, λ is the centroid wavelength, T is the temperature, and c_2 is the second radiation constant. The uncertainties are divided between those associated with the radiation thermometer and those associated with the gold freezing temperature blackbody and its operation. The dominant term in the uncertainty budget is the long-term stability of the radiation thermometer in row 2. This component was assigned from the average 0.1%/year drift, since its construction, of the AP1 observed from repeated gold-point measurements.

4 Measurement of Gold Freezing Temperatures

The results of the AP1 gold freezing temperature measurements, in 2005 and 2007, are shown in Table 7 along with the TRT650 measurement. The detector-based radiation

Table 6 Uncertainty components of the AP1 and the TRT650 for the Au freezing-temperature determinations

	Signal uncertainty component	($k = 1$) (%)
1	Spectral radiance responsivity	0.032
2	Temporal stability of responsivity	0.050
3	Plateau identification	0.005
4	Emissivity	0.010
5	Preamplifier gain	0.025
6	Dark current drift	0.015
7	Size-of-source effect	0.010
	Total uncertainty in signal	0.068
	Expanded uncertainty ($k = 2$)	0.135
	Temperature uncertainty (K) ($k = 2$)	0.109

Table 7 Measurements of the gold freezing temperature blackbody with the respective radiation thermometers compared to the ITS-90 temperature

Radiation thermometer	Date, gold-point measurement	Date, SIRCUS calibration	T (K)	$T - T_{90}$ (K)
AP1	August 2005	June 2005	1337.49	0.16
AP1	March 2007	November 2006	1337.65	0.32
TRT650	March 2007	November 2006	1337.52	0.19

The differences, $T - T_{90}$, are outside the calculated uncertainty of the temperature determination of 0.109 K ($k = 2$)

thermometer signals were corrected prior to the determination of temperatures using Eq. 2 by

$$i = G\frac{\sigma}{\varepsilon}i_{\mathrm{m}}, \tag{5}$$

where i_{m} is the measured photocurrent, i is the corrected photocurrent, G is the gain correction factor, ε is the emissivity, and σ is the SSE correction. The temperatures were found using the corrected photocurrents from Eq. 5 applied to the calculated photocurrents in Fig. 5.

5 Measurement of VTBB Temperatures

5.1 Nonlinearity of the AP1

In addition to the gold freezing temperature measurements, the temperature of the TGBB was determined from 800 to 2,700°C using the NIST PEP, the AP1, and the TRT650. The initial measurements revealed that $T - T_{90}$ agreed within the combined uncertainties, but the AP1 temperatures deviated from the TRT650 and PEP measurements at T>2,100°C. This deviation was further explored by plotting the ratios of the photocurrents of the AP1 and the TRT650, as shown in Fig. 7. Such signal ratios can be utilized since both radiation thermometers utilize the same interference filter at 650 nm. The signal ratios are constant from 10^{-10} to 10^{-7} A, but above 10^{-7} A, the

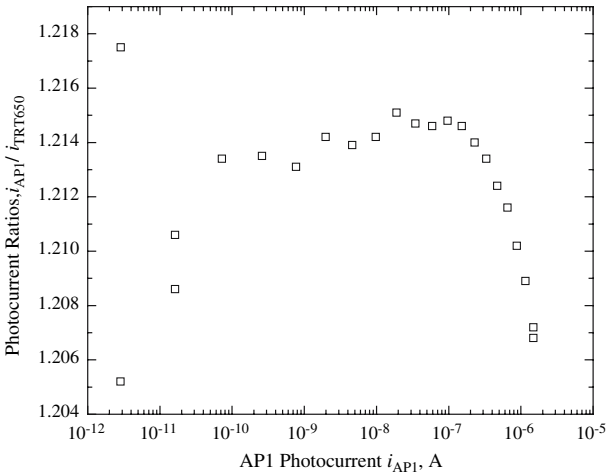

Fig. 7 Photocurrent ratios, i_{AP1}/i_{TRT650}, plotted against the AP1 photocurrent show constant ratios from 1×10^{-10} to 1×10^{-7} A, indicating linear behavior over this region. Nonlinearity is evident from the rapid fall off past 1×10^{-7} A. Scatter in the ratios at AP1 photocurrents $<1 \times 10^{-10}$ A is due to the noise in the signals

AP1 signals are lower than the TRT650 signals. We examined the time-dependent AP1 signals, with the TGBB at 2,700°C, to determine if there were any time-dependent changes due to thermal heating, as might arise from changes in the throughput or from filter changes leading to lower measured photocurrents. The AP1 signals with the TGBB were found to be stable with time. We also replaced preamplifiers to determine if the current-to-voltage conversion was incorrect. The preamplifier outputs were comparable, within the combined uncertainty of $<0.08\%$ ($k = 2$).

Since there were no time-dependent changes to the AP1 signal at these photocurrent levels and blackbody temperatures, the deviations could originate from the nonlinearity of the photodiode. Although, in typical applications, nonlinearity of the Si diode is expected to be present at optical power levels near 1 mW or greater, a possible reason for the onset of nonlinearity at lower power levels could be from the overfilled illumination of the Si diode. Such sources of nonlinearity with overfilled illumination have been observed in radiation thermometers utilizing InGaAs detectors [18,19]. In InGaAs and Ge diodes, radiation, which is incident outside the active area, leads to possible capture by defect states, thus leading to nonlinear responsivities. To test for these effects, the area of the aperture stop of the AP1 was reduced by 60%, resulting in f/15.5. As shown in Fig. 8, the ratios of signals from the AP1 and the TRT650 are plotted as a function of AP1 photocurrent. The AP1 signals, with the restricted aperture stop of f/15.5, display lower nonlinearities than the signals measured at f/12, but the nonlinearities are not completely eliminated by this modification. Further studies are needed to quantify the dependence of the linearity on illumination conditions.

5.2 Nonlinearity-Corrected AP1 Temperatures

The results of the temperature measurements using the AP1, TRT650, and the PEP are shown in Fig. 9 as temperature differences, $T - T_{90}$. The PEP temperatures are

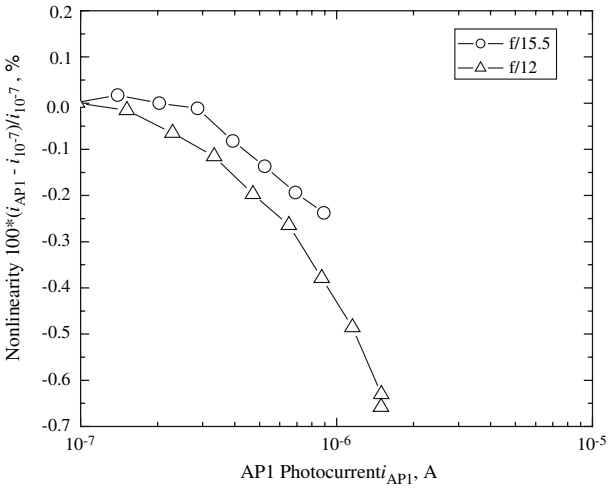

Fig. 8 Comparison of the nonlinearity found for f/12 versus f/15.5. The larger f/# was achieved by restricting the aperture stop with the placement of an iris at the objective lens. The smaller illumination area on the detector, away from the edges, leads to a reduction in the nonlinearity

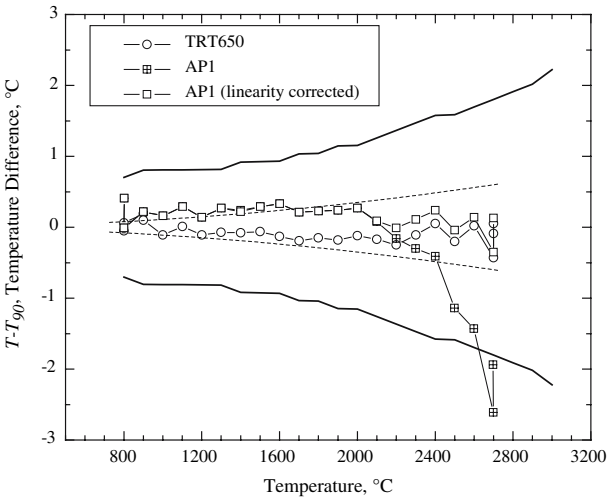

Fig. 9 Temperature differences, $T - T_{90}$, of the AP1 (both uncorrected and corrected for linearity) and the TRT650 from the ITS-90 based PEP measurements. Thin dashed lines denote the detector-based expanded temperature uncertainties ($k = 2$), and the thick solid lines denote the ITS-90-based PEP temperature uncertainties ($k = 2$). The linearity corrected AP1 temperatures are in agreement with the TRT650 temperatures within the combined uncertainties

determined by radiance ratios with respect to a stable, vacuum tungsten-strip lamp, which was, in turn, assigned a radiance temperature from the gold freezing point. The AP1 and the TRT650 temperatures are assigned from the detector-based radiation thermometry. The increase in the differences at 800°C for the AP1 is due, in part, to the low signals being measured. The improved performance of the TRT650 can be

observed at 800°C, where the reproducibility is assisted by the low-noise performance of the preamplifier. In the temperature region from 900 to 2,400°C, the $T - T_{90}$ differences are within the larger PEP uncertainties and just outside the expanded ($k = 2$) uncertainties of the two detector-based radiation thermometers. Above 2,400°C, the TRT650 temperatures are in agreement with the PEP assigned temperature, but the AP1 assigned temperatures are lower than the PEP and the TRT650 temperatures well outside the expanded uncertainties. This deviation was observed in past studies [20], and is now attributed to nonlinearity of the AP1 with illumination of the Si photodiode outside the active region. If the AP1 nonlinearity is corrected using the radiance ratios of the TRT650 and the PEP from 10^{-10} A and 10^{-7} A to the AP1 photocurrents $>10^{-7}$ A, the AP1 temperatures are in agreement with both the TRT650 and the PEP measurements.

6 Discussion

Using the AP1, with the repeated determinations of the detector-based radiance responsivities from SIRCUS along with the repeated measurements of the gold freezing temperature blackbody, we are able to demonstrate that the low, stated uncertainties can be maintained. The small drift of the AP1 determination of the gold freezing temperature outside the stated uncertainties reveals that the detector-based calibration should be closely followed by the freezing-point measurements. The slightly higher gold freezing temperatures of the AP1 and the TRT650 are within the combined uncertainties of the ITS-90 thermodynamic temperature uncertainties and the detector-based responsivity calibrations.

The comparisons with the TRT650 have shown the limitation of the AP1 with respect to linearity at higher photocurrents and preamplifier noise performance at very low photocurrents. The lack of a final detector mask on the AP1 has led to unexpected nonlinearity issues. The TRT650 has a mask in front of the diode that limits the radiation to the active area. Furthermore, the AP1 was constructed prior to our SSE studies, which showed the importance of the low-scatter objective and the Lyot stop, and suffers from relatively high SSE as compared to the TRT650. Although the AP1 will be modified to further understand the nonlinearity issues of the Si diode, further studies and development of the thermodynamic temperature scale will be performed with the TRT650.

We are in the process of developing additional portable radiation thermometers centered at 650 nm designed for international temperature comparisons. Such radiation thermometers will be tested for nonlinearity as a system and also designed with diode masks to avoid illumination away from the active region.

The TRT650 radiation thermometer will be used routinely in the NIST Radiance Temperature Calibration Laboratory alongside the PEP radiation thermometer. The measurements of the tungsten-strip lamp with the TRT650 will determine both the short- and long-term stability of the detector-based radiation thermometer and its suitability for use in routine calibrations. With sufficient data collected after several months of use alongside the PEP, a decision will be made whether further improvements to the TRT650 are needed or thermodynamic temperatures will be directly disseminated.

7 Conclusions

We have described the construction, characterization, and the use of the new NIST TRT. The performance of this new radiation thermometer is compared with the AP1 and the PEP, and found to be in agreement within the combined uncertainties. A nonlinear behavior of the AP1 at photocurrents $>1 \times 10^{-7}$ A has been found and attributed to overfilling of the photodiode. The linearity-corrected AP1 temperatures agree with the TRT650 and the PEP within the combined uncertainties. These results show that NIST is ready to begin issuing thermodynamic temperature scales above 800°C in accordance with the anticipated redefinition of the kelvin based upon a fixed value of the Boltzmann constant.

References

1. I.M. Mills, P.J. Mohr, T.J. Quinn, B.N. Taylor, E.R. Williams, Metrologia **43**, 227 (2006)
2. B. Fellmuth, Ch. Gaiser, J. Fischer, Meas. Sci. Technol. **17**, R145 (2006)
3. *Supplementary Information for the International Temperature Scale of 1990*, Bureau International des Poids et Mesures, Sèvres (1990)
4. L. Ma, F. Sakuma, in *Proceedings of the Society of Instrument and Control Engineers Annual Conf.*, SICE04 (2004), pp. 323–328
5. H.C. McEvoy, G. Machin, R. Friedrich, J. Hartmann, J. Hollandt, in *Temperature: Its Measurement and Control in Science and Industry*, vol. 7, ed. by D.C. Ripple (AIP, New York, 2003), pp. 909–914
6. H.W. Yoon, D.W. Allen, C.E. Gibson, M. Litorja, R.D. Saunders, S.W. Brown, G.P. Eppeldauer, K.R. Lykke, Appl. Optics **46**, 2870 (2007)
7. N.P. Fox, J.E. Martin, D.H. Nettleton, Metrologia **28**, 221 (1991)
8. M. Noorma, P. Karha, T. Jankowski, F. Manoocheri, T. Weckstrom, L. Uusipaikka, E. Ikonen, in *Proceedings TEMPMEKO 2004, 9th International Symposium on Temperature and Thermal Measurements in Industry and Science*, ed. by D. Zvizdić, L.G. Bermanec, T. Veliki, T. Stašić (FSB/LPM, Zagreb, Croatia, 2005), pp. 101–106
9. D.R. Taubert, J. Hartmann, J. Hollandt, J. Fischer, in *Temperature: Its Measurement and Control in Science and Industry*, vol. 7, ed. by D.C. Ripple (AIP, New York, 2003), pp. 7–12
10. S.W. Brown, G.P. Eppeldauer, K.R. Lykke, Appl. Optics **45**, 8218 (2007)
11. D.W. Allen, R.D. Saunders, B.C. Johnson, C.E. Gibson, H.W. Yoon, in *Temperature: Its Measurement and Control in Science and Industry*, vol. 7, ed. by D.C. Ripple (AIP, New York, 2003), pp. 577–582
12. C.E. Gibson, B.K. Tsai, A.C. Parr, *NIST Special Pub. 250-43* (U.S. Government Printing Office, Washington, 1998)
13. D.W. Allen, G. Dezsi, H.W. Yoon, in *Proceedings TEMPMEKO 2004, 9th International Symposium on Temperature and Thermal Measurements in Industry and Science*, ed. by D. Zvizdić, L. G. Bermanec, T. Veliki, T. Stašić (FSB/LPM, Zagreb, Croatia, 2005), pp. 817–822
14. H.W. Yoon, D.W. Allen, R.D. Saunders, Metrologia **42**, 89 (2005)
15. H.W. Yoon, C.E. Gibson, V. Khromchenko, G.P. Eppeldauer, SSE- and Noise-Optimized InGaAs Radiation Thermometer, in *Proceedings TEMPMEKO 2007* (to be published in Int. J. Thermophys.). doi: 10.1007/s10765-007-0309-5
16. P.J. Mohr, B.N. Taylor, Rev. Mod. Phys. **77**, 1 (2005)
17. N. Sasajima, C.E. Gibson, V. Khromchenko, R.D. Saunders, H.W. Yoon, *Proceedings of the 9th international Conference on New Developments and Applications in Optical Radiometry* (NEWRAD), ed. by J. Grobner (Davos, Switzerland, 2005), pp. 327–328
18. M. Battuello, F. Girard, T. Ricolfi, in *Proceedings TEMPMEKO 2004, 9th International Symposium on Temperature and Thermal Measurements in Industry and Science*, ed. by D. Zvizdić, L.G. Bermanec, T. Veliki, T. Stašić (FSB/LPM, Zagreb, Croatia, 2005), pp. 505–508
19. P. Corredera, M.L. Hernanz, M. González-Herráez, J. Campos, Metrologia **40**, S150 (2003)

20. C.E. Gibson, D.W. Allen, G.P. Eppeldauer, H.W. Yoon, in *Proceedings TEMPMEKO 2004, 9th International Symposium on Temperature and Thermal Measurements in Industry and Science*, ed. by D. Zvizdić, L.G. Bermanec, T. Veliki, T. Stašić (FSB/LPM, Zagreb, Croatia, 2005), pp. 127–132